ARTICLES
PUBLISHED ONLINE: 21 MARCH 2010 | DOI: 10.1038/NPHYS1613
nature physics

Optimal matrix rigidity for stress-fibre polarization in stem cells

A. Zemel[1]*†, F. Rehfeldt[2,3]†, A. E. X. Brown[2], D. E. Discher[4] and S. A. Safran[5]

The shape and differentiated state of many cell types are highly sensitive to the rigidity of the microenvironment. The physical mechanisms involved, however, are unknown. Here, we present a theoretical model and experiments demonstrating that the alignment of stress fibres within stem cells is a non-monotonic function of matrix rigidity. We treat the cell as an active elastic inclusion in a surrounding matrix, allowing the actomyosin forces to polarize in response to elastic stresses developed in the cell. The theory correctly predicts the monotonic increase of the cellular forces with the matrix rigidity and the alignment of stress fibres parallel to the long axis of cells. We show that the anisotropy of this alignment depends non-monotonically on matrix rigidity and demonstrate it experimentally by quantifying the orientational distribution of stress fibres in stem cells. These findings offer physical insight into the sensitivity of stem-cell differentiation to tissue elasticity and, more generally, introduce a cell-type-specific parameter for actomyosin polarizability.

Recent research has shown that the regulation of important cellular processes, such as proliferation, differentiation and apoptosis, is controlled by the mechanical properties and geometry of the cells and their environment[1–11]. Cell differentiation and other cellular processes have been shown to reach an optimum in a range of matrix rigidities that is characteristic of the native tissue environment[4–8]; the rigidity of the environment can direct the shape and lineage specification of human mesenchymal stem cells[7] (hMSCs). When plated on substrates with a rigidity that mimics that of brain, muscle and bone, stem cells expressed differentiation markers corresponding to these tissue cells after a few days and showed maximum expression on the respective substrates. Significant differences in cell morphology, however, emerge within the first 24 h. The extent of cell elongation (aspect ratio) depended non-monotonically on the rigidity of the matrix[7], adopting the characteristic polarized morphology of muscle cells only when placed on a matrix with a rigidity that matched the typical stiffness of muscle tissue ($E \approx 10$ kPa).

Here, we focus on the alignment of the contractile, actomyosin stress fibres in the cytoskeleton of adhering cells (Fig. 1) because they were shown to have an essential role in the active, mechanosensitivity of cells[12], particularly in the determination of cell shape[13] and differentiation[14]. We predict theoretically and demonstrate experimentally that the matrix rigidity and the cell shape regulate the polarization of stress fibres in cells, and dictate the preferential alignment of the stress fibres along the long axis of the cell[15–17]. We show that the alignment of stress fibres in stem cells depends non-monotonically on the matrix rigidity, attaining a maximum value when the cell and matrix rigidity are similar.

We model the cell as an active, elastic inclusion in an infinite, homogeneous and isotropic medium and consider both two-dimensional (2D) and 3D geometries. The theory includes both the passive forces arising from the elasticity of the cell and the surrounding medium as well as the active forces generated and regulated by the cells; this extends the treatment of passive inclusions in solids to living matter. We show that a small asymmetry in the early-time shape of an adhering cell (see Supplementary Fig. S2) results in a symmetry breaking of the elastic stress in the cell that in turn, may direct the spontaneous polarization of the stress-fibres in the cell. We invoke the use of an active cell polarizability that reflects the feedback between the elastic stresses in the cell and the active forces that the cell generates to predict the anisotropic polarization of the forces in the cell and its dependence on the cell shape and elastic characteristics.

Experiments were carried out to systematically analyse the alignment of stress fibres in hMSCs as a function of the cell shape and the rigidity of the environment. Cells were cultured on substrates of varying stiffness and sorted by their aspect ratio. We show a quantitative analysis of stress-fibre polarization in cells by staining for both actin and non-muscle myosin IIa (NMMIIa) and applying a segmentation algorithm to map their spatial organization in the cell.

Our results suggest a generic mechanical coupling between the cell shape, the rigidity of the surroundings and the organization of stress fibre in the cytoskeleton of stem cells. This identifies a mechanical property of cells—stress-fibre polarization—that is maximized at an optimal substrate rigidity, analogous to the optimal rigidity found in stem-cell differentiation (for example, to muscle cells).

Theory of cell adhesion and actomyosin polarization

The anchoring of a cell to the extracellular matrix as well as the active spreading of a cell on a surface involves a shape and volume deformation that produces elastic stresses in the cell and the matrix[17–22]. Nascent protein adhesion complexes (often termed focal complexes[12]) that anchor the cell to the surrounding matrix grow in response to these forces[23] providing mechanical support for stronger, organized and more prominent actomyosin stress fibres in the cell. The theory shows how the adhesion-induced stresses can initiate a feedback that controls the amount and alignment of the

[1]Institute of Dental Sciences, Faculty of Dental Medicine, and the Fritz Haber Center for Molecular Dynamics, the Hebrew University-Hadassah Medical Center, Jerusalem 91120, Israel, [2]Department of Physics and Astronomy, University of Pennsylvania, Philadelphia, Pennsylvania 19104, USA, [3]III. Physikalisches Institut, Georg-August-Universität, 37077 Göttingen, Germany, [4]Graduate Group of Physics and Astronomy, University of Pennsylvania, Philadelphia, Pennsylvania 19104, USA, [5]Department of Materials and Interfaces, Weizmann Institute of Science, Rehovot 76100, Israel. †These authors contributed equally to this work. *e-mail: assaf.zemel@ekmd.huji.ac.il.

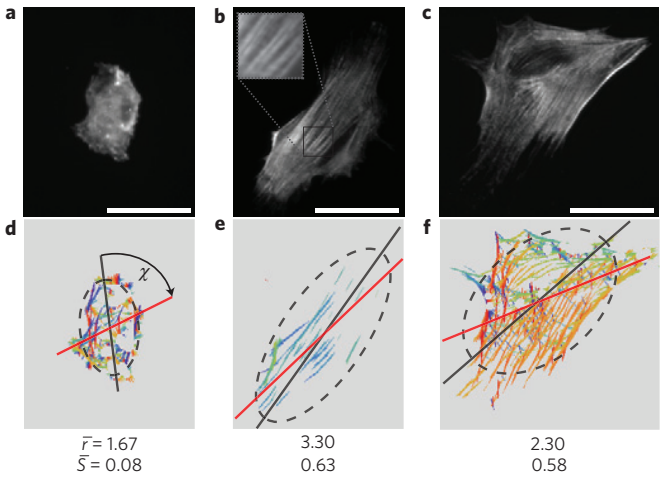

Figure 1 | Actomyosin stress-fibre alignment in hMSCs sparsely plated on 2D substrates of different elasticities. a–c, hMSCs immunostained for myosin NMMIIa 24 h after plating on elastic substrates with Young's moduli E_m of 1 (**a**), 11 (**b**) and 34 kPa (**c**). Images are the most representative cells of the mean values obtained for cell area A, aspect ratio of long to short axis r and stress-fibre order parameter $S = \langle \cos 2\theta \rangle$, where θ is the angle between each stress fibre in the cell and the long axis of the fitted ellipse. **d–f**, The respective orientational plots, where the different orientations of myosin filaments are depicted with different colours. The dark grey dashed ellipses are calculated from the moments up to the second order and represent the cell shape in terms of area and long and short axes, and the red line indicates the mean orientation of the stress fibres as determined by the anisotropic filter algorithm. χ is the angle between the mean stress-fibre orientation and the principal axis of the ellipse. From symmetry considerations, we need consider only the absolute value of χ between 0 and $\pi/2$; thus, a completely random distribution has an average $\chi = \pi/4$. Values given for r and S are the mean values of at least 60 cells per condition. All scale bars represent 50 μm.

stress fibres in the cell; we begin with a simple 1D spring model[24] and then extend it in full elastic 2D and 3D models.

In the spring model (Fig. 2), the passive elasticities of the cell and the matrix are represented by springs with rigidities, k_c and k_m, respectively. We denote by l_c^R the relaxed length of the cellular spring as it would exist in a soft environment of vanishing rigidity. This length is determined, in part, by active forces, f^0 (not shown in Fig. 2), arising from the initial, isotropic distribution of myosin motors that locally compresses the cytoskeleton. We begin with the first stage of cell adhesion (Fig. 2a–b) where the cell anchors to the matrix or spreads isotropically[18] on a surface and an elastic stress develops in the cell. Experiments show that the spreading area and the force exerted by cells increase with the matrix rigidity[4,6,16,25]. We denote by $-\Delta l_c^0 = l_c^0 - l_c^R > 0$ the elastic deformation that would arise if the cellular springs were maximally stretched, as appropriate to spreading on a substrate of infinite rigidity, where l_c^0 denotes the fully stretched size of the cellular spring as it exists in an infinitely rigid matrix.

We now consider the equilibrium spring lengths, l_c and l_m, including the matrix deformation, but not yet including the feedback that leads to well-developed actomyosin stress fibres (Fig. 2b) (this latter step typically begins tens of minutes after cell spreading[9] and lasts for many hours). To calculate the equilibrium spring lengths we solve the force balance equation: $k_c(l_c - l_c^R) = k_m(l_m - l_m^R)$ along with the (boundary) condition $l_c + l_m = l_c^0 + l_m^R$; here l_m^R is the equilibrium length of the matrix spring. This results in the following relation: $\Delta l_c = [k_c/(k_c + k_m)]\Delta l_c^0$, where $\Delta l_c = l_c - l_c^0$.

A simple feedback mechanism is next included in which the modulation of the active actomyosin force exerted by the cell,

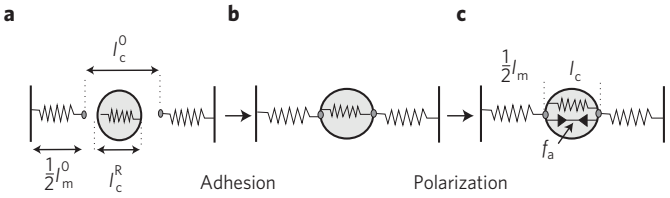

Figure 2 | Cell adhesion and polarization represented by a 1D spring model. Springs with constants k_c and k_m represent the elasticity of the cell and matrix respectively. Elastic morphological changes on cell adhesion (**a–b**) are represented here by a change in the cellular spring length $\Delta l_c = [k_c/(k_c + k_m)]\Delta l_c^0$ This triggers an internal feedback mechanism (**b–c**) that results in an enhancement of the active forces (see equation (2)), and to a further change in cell length as given by equation (1).

$f^a = f - f^0$, resulting from the assembly of organized anisotropic stress fibres in the cell, is proportional to the stress within the cell; f is the total actomyosin force. We write this feedback as follows: $f^a = -\alpha k_c(l_c - l_c^R) = -\alpha k_c(\Delta l_c - \Delta l_c^0)$. Here, $\alpha > 0$ is a phenomenological 'polarizability' that relates the stress in the cytoskeleton to the number, size and orientation of the stress fibres and focal adhesions in the cell. In the presence of these active forces, the force balance equation reads: $k_c(l_c - l_c^R) = k_m(l_m - l_m^R) + f^a$. This enables us to predict the magnitude of the average force and strain that develop in a cell as a function of the cell and matrix rigidity (Fig. 2c). For the cellular strain we find:

$$\frac{\Delta l_c}{l_c^0} = \frac{\tilde{k}_c}{(\tilde{k}_c + k_m)} \frac{\Delta l_c^0}{l_c^0} \tag{1}$$

Here, $\tilde{k}_c = (1 + \alpha)k_c$ is the effective rigidity of the cell; an active cell is effectively more rigid (for $\alpha > 0$) because the stretching by the matrix springs enhances the active contractile forces in the cell, which further oppose the matrix stretch. In addition, the net, anisotropic polarized actomyosin force is given by:

$$\frac{f^a}{f^0} = \alpha \frac{k_m}{\tilde{k}_c + k_m} \tag{2}$$

This expression correctly captures the experimentally observed monotonic increase and saturation of the contractile cellular force with the matrix rigidity, see Supplementary Fig. S3 and ref. 16.

The 1D spring model is useful for understanding the increase in cell contractility but is unable to account for the anisotropic polarization of the forces in the cell. To this end, we use approaches from solid mechanics, and generalize the well-known inclusion problem[26,27] to include the 'live' nature of cells, that is their ability to actively regulate their forces. We do this both for 2D and 3D systems; see Supplementary Information for details.

We model the cell as an isotropic and homogeneous ellipsoid embedded in an infinite 3D matrix; the same formalism applies to an elliptical cell embedded in a 2D sheet under conditions of generalized plane stress[28,29]. We denote by $\mathbf{C}_c$ and $\mathbf{C}_m$ the mean elastic moduli of the cell and the matrix, respectively. Bold face letters are used to designate fourth-rank tensors and a product of the form $\mathbf{A}g_{ij}$ denotes $A_{ijkl}g_{kl}$, and similarly $\mathbf{AB}g_{ij} = A_{ijmn}B_{mnkl}g_{kl}$, where summation over repeated indices is implied. The isotropic modulus, $\mathbf{C}_c$, refers to the cell elasticity on adhesion, as it exists before the stress fibres have become numerous and oriented; this includes contributions from other cytoskeletal components and from actin that is in an isotropic, gel state. We denote by $-u_{ij}^0 > 0$ the early-time strain associated with cell adhesion and spreading in an infinitely rigid environment (analogous to $-\Delta l_c^0$ in the spring model); this produces a restoring stress $\mathbf{C}_c u_{ij}^0 < 0$ in the cytoskeleton that initiates the polarization response.

The active actomyosin forces in the cytoskeleton are modelled by a local distribution of 'force dipoles'[30–32] that arise from the equal and opposite forces exerted by myosin motors at two nearby points on actin filaments. These are represented by a tensor quantity $\langle p_{ij}\rangle$, which is the average (active) dipole density per unit volume. We assume that these force dipoles polarize in response to the local stress in the cell, changing their magnitude and orientation from their average, isotropic initial value $\langle p^0_{ij}\rangle$. We denote by $\langle p^a_{ij}\rangle = \langle p_{ij}\rangle - \langle p^0_{ij}\rangle$, the anisotropic polarization tensor of the force dipoles in the cytoskeleton and in analogy to the spring model, we assume a feedback response of the form:

$$\langle p^a_{ij}\rangle = -\boldsymbol{\alpha}\mathbf{C}_c(u^c_{ij} - u^0_{ij}) \tag{3}$$

where $\boldsymbol{\alpha}$ denotes the active cellular polarizability (see Supplementary Information) and $\mathbf{C}_c(u^c_{ij} - u^0_{ij})$ is the mean stress developed in the cell[26]. The strain and the forces that develop in the cell because of this feedback response are given by the self-consistent solution of the elastic equations along with the feedback effect of equation (3). This predicts that the strain and the cell force are given by:

$$u^c_{ij} = [\widetilde{\mathbf{A}}(\mathbf{S}_m - \mathbf{I}) + \mathbf{I}]u^0_{ij} \tag{4}$$

and

$$\langle p^a_{ij}\rangle = -\boldsymbol{\alpha}\mathbf{C}_c\widetilde{\mathbf{A}}(\mathbf{S}_m - \mathbf{I})u^0_{ij} \tag{5}$$

with $\widetilde{\mathbf{A}} = [\mathbf{I} + \mathbf{S}_m(\widetilde{\mathbf{C}}_c - \mathbf{C}_m)\mathbf{C}_m^{-1}]^{-1}$; $\mathbf{I}$ is the unit tensor. The quantity $\widetilde{\mathbf{C}}_c = (\mathbf{I}+\boldsymbol{\alpha})\mathbf{C}_c$ is the effective elastic modulus of the cell (analogous to $\widetilde{k}$ in the spring model). This tensor embodies the 'live' properties of cells through the cell polarizability, $\boldsymbol{\alpha}$. The tensor, $\mathbf{S}_m$, is the Eshelby tensor[26,27], a function of the cell shape and the Poisson ratio of the matrix. Equations (4) and (5) (which generalize equations (1) and (2) of the spring model) allow us to explore the relationship between the cell shape and the polarization of the forces, and to predict how anisotropic stress fibres first arise. The establishment of cell shape and polarization of stress fibres occur on a timescale of hours to days, during which the elastic properties of cytoskeleton and cell shape vary. However, the final steady state of the cell emerges from an early-time breaking of symmetry, the origin and mechanical consequences of which are described by our model.

Predictions and experimental observations

Experimentally, focal adhesions and stress fibres have been shown to grow and develop parallel to the direction of an applied force[33], consistent with the more general observation that cells tend to polarize in the direction of stronger elastic resistance[34]. We thus consider the simplest model in which a cell responds to stresses by locally modulating its active actomyosin forces only in directions parallel to the local stress. In this case, the isotropic fourth-rank tensor, $\boldsymbol{\alpha}$, can be replaced by a single positive scalar quantity, α, and $\langle p^a_{ij}\rangle = -\alpha\mathbf{C}_c\Delta u^c_{ij}$ (see equation (3)). In the Supplementary Information we discuss an alternative form for $\boldsymbol{\alpha}$, but the conclusions of the main body of the article are unaltered in that model as well.

To illustrate how the shape of the cell alone can be responsible for the polarization anisotropy, we assume, for simplicity, and in line with experiments[18] that the initial-time adhesion-induced stress, $\mathbf{C}_c u^0_{ij}$, is isotropic, including the contribution arising from the early-time force dipoles, $\langle p^0_{xx}\rangle = \langle p^0_{yy}\rangle = \langle p^0_{zz}\rangle = p^0$. Nevertheless, the global shape change (elongation of the cell) that accompanies the polarization of stress fibres in the cell may involve further axial stretching of the cytoskeleton. This effect is considered below, but we first focus on the consequences of the isotropic forces exerted by the cell. Although the actual proportion of isotropic dipolar forces, $\langle p^0_{ij}\rangle$, in the total stress exerted by the cell, $\mathbf{C}_c u^0_{ij}$, is unknown, for simplicity, and without loss of generality we use

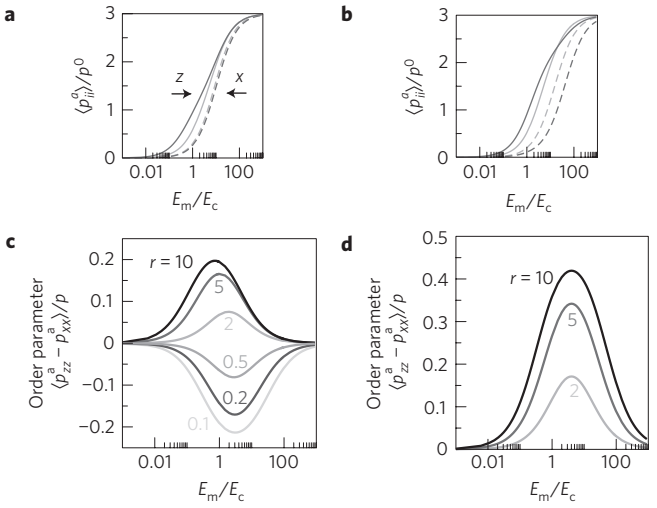

Figure 3 | Cell polarization as a function of the ratio of Young's modulus of the matrix, E_m, and the cell, E_c, in both our 2D and 3D models. The plots are shown for different values of the cellular aspect ratio, r. **a**,**b**, The normalized average dipole elements $\langle p^a_{zz}\rangle$ (solid lines) and $\langle p^a_{xx}\rangle$ (dashed lines) corresponding to the forces in the directions that are respectively parallel ($\hat{z}$) and perpendicular ($\hat{x}$) to the long axis of the cell (dark grey: $r = 5$, light grey: $r = 2$) for our 3D (**a**) and 2D (**b**) models. **c**,**d**, The calculated orientational order parameter of the stress fibres that is given by the normalized difference $(\langle p^a_{zz}\rangle - \langle p^a_{xx}\rangle)/p$ for our 3D (**c**) and 2D (**d**) models. The colour coding indicates the aspect ratio. In this plot, the Poisson ratio of the matrix and the cellular domain are taken to be $\nu_m = 0.45$ and $\nu_c = 0.3$ and the magnitude of the polarizability is $\alpha = 3$.

$\mathbf{C}_c u^0_{ij} = \langle p^0_{ij}\rangle$ in the calculations presented below. We model cells in 3D as spheroids with long-axis (taken to be in the z direction) length c and short-axis (taken to be in the x–y plane) radius a. Similarly, in our 2D model the cell is modelled by an ellipse with long and short axes c and a respectively; in both cases $r = c/a$ is the aspect ratio of the cell.

Figure 3 shows our results for both the 2D and 3D systems. Figure 3a,b shows the normalized dipole elements $\langle p^a_{zz}\rangle/p^0$ and $\langle p^a_{xx}\rangle/p^0$, as a function of the ratio of Young's modulus of the matrix and the cell, E_m/E_c, for two values of the aspect ratio r. Consistent with experiment[16], our 1D spring model and our estimate of the total myosin content in the stress fibres (Supplementary Fig. S3), we find that the magnitude of the cellular forces in both the x and z directions increases monotonically with the rigidity of the matrix up to the same saturation value, $\langle p^a_{zz}\rangle/p^0 = \langle p^a_{xx}\rangle/p^0 = \alpha$. For intermediate values of the matrix rigidity, the matrix tractions that oppose the cellular forces turn out to be stronger along the long axis of the cell. This fact, which is entirely due to the anisotropic shape of the cell, is responsible for the stronger polarization of the forces along the long axis of the cell. Thus, for rod-like cells oriented parallel to the z axis, we find that $\langle p^a_{zz}\rangle > \langle p^a_{xx}\rangle$. The preferential alignment of stress fibres (as well as of the sarcomeres in muscle cells) parallel to the long axis of cells is a common experimental observation[15–17], which has not been explained theoretically.

Our theory shows that the polarization of the stress fibres in the cell should depend non-monotonically on the matrix rigidity. To illustrate this behaviour, Fig. 3c,d plots the normalized difference, $S = (\langle p_{zz}\rangle - \langle p_{zz}\rangle)/p = (\langle p^a_{zz}\rangle - \langle p^a_{xx}\rangle)/p$, which can be shown to be equal to the orientational order parameter of the dipoles; here p is the trace of the mean dipole tensor, $\langle p_{ij}\rangle$. In both 2D and 3D we find the same, generic, Lorentzian type (that is, a Lorentzian multiplied by the linear factor E_m/E_c) of functional dependence for S as a function of Young's moduli ratio: $S = a(E_m/E_c)/[b((E_m - E_0)/E_c)^2 + 1]$, where a, b, E_0 are complicated

functions of the aspect ratio, cell polarizability, Poisson ratio of the cell and matrix and dimensionality of the system.

We find that the polarization of the forces in the cell is maximal at an optimal ratio of the matrix and cell rigidities, $(E_m/E_c)^\star$. The explanation for this important feature is as follows. Consider the two extreme limits of a cell in an infinitely rigid and infinitely soft matrix. In the former case, because the matrix exerts strong tractions that completely oppose the initial, isotropic, inward pulling forces of the cell, $f_i^0 = \mathbf{C}_c u_{ij}^0 n_j$, the early-time (tensile) stress that develops, $\mathbf{C}_c(u_{ij}^{c,0} - u_{ij}^0) = -\mathbf{C}_c u_{ij}^0$, is also isotropic (see Supplementary Equation (6)); this results in an isotropic polarization of the stress fibres because $\langle p_{ij}^a \rangle = \sigma_{ij}^c/\alpha$ (where $\sigma_{ij}^c = \mathbf{C}_c(u_{ij}^c - u_{ij}^0)$). In the opposite limit of an infinitely soft matrix, the matrix resistance, and consequently the cellular stress, drops to zero in all directions, thus providing no orientational cue for the polarization of stress fibres in the cell. Between these two limits, the forces in different directions increase with different rates with the matrix rigidity as seen in Fig. 3a,b. As the saturation values are independent of direction, the difference in the polarization, parallel and perpendicular to the long axis of the cell, has a maximum at a certain value of the matrix rigidity.

Interestingly, we predict that the optimal ratio, $(E_m/E_c)^\star$, scales as $\sim\sqrt{1+\alpha}$ (see Supplementary Information). As α is, in general a cell-type-specific parameter, this scaling suggests that different cell types would possess a different level of sensitivity to the anisotropy of the stress in the cell. In addition, our theory shows that the stress-fibre polarization in 2D is larger by a factor of $\approx$2 compared with 3D. In 3D the cell is surrounded by a matrix that more strongly suppresses the anisotropy of the elastic stress in the cell. In the Supplementary Information we present a more quantitative analysis of these arguments.

Thus far we considered the sole effect of the stress anisotropy that results from the cell shape. This gives rise to a non-monotonic dependence of stress-fibre polarization on the matrix rigidity. The stress-fibre polarization however is often accompanied by a simultaneous narrowing and elongation of the cell; see Fig. 1. To model the consequences of the stress associated with cell elongation we include an axial contribution to the early-time elastic stress $\mathbf{C}_c u_{ij}^0$ exerted by the cell and calculate its effect on the polarization of stress fibres in the cell. We note that this is an approximation because the cell shape changes continuously but nevertheless it captures an important elastic consequence of cell spreading anisotropy. We thus write $\mathbf{C}_c u_{ij}^0 = p^0(\delta_{ij} + \eta\delta_{iz}\delta_{jz})$, where the second term is an axial stress along the z axis—the direction of cell elongation. Like the separate elements of the stress tensor σ_{xx}^c and σ_{zz}^c in the previous case, the stress resulting from this axial contribution increases with the matrix rigidity. Figure 4a shows the predicted effect of this axial stress on the polarization of the stress fibres in the cell. Rather than dropping to zero as the matrix rigidity increases, the order parameter saturates to a finite value given by $\eta\alpha/(\eta\alpha + d + d\alpha)$, where $d = 2, 3$ is the dimensionality.

To test the predictions of our model we imaged actin and NMMIIa in hMSCs sparsely grown on substrates of different elasticities (Fig. 1a–c). The overall aspect ratio r of the cell and the orientation of the contractile stress fibres have been determined; to quantify the polarization response we calculated the order parameter $S = \langle\cos 2\theta\rangle$, where θ is the angle between each stress fibre in the cell and the long axis of the fitted ellipse. See the Methods section for details.

Cells imaged 1 h after plating on the substrate showed aspect ratios, r, slightly greater than unity (see Supplementary Fig. S2), and although some stress fibres had already developed, there was no significant polarization, yielding order parameters S close to zero. This situation changes 4 h after plating the cells; the order parameter S increases and shows a non-monotonic behaviour as a function of the matrix rigidity, as shown in the inset of Fig. 4b.

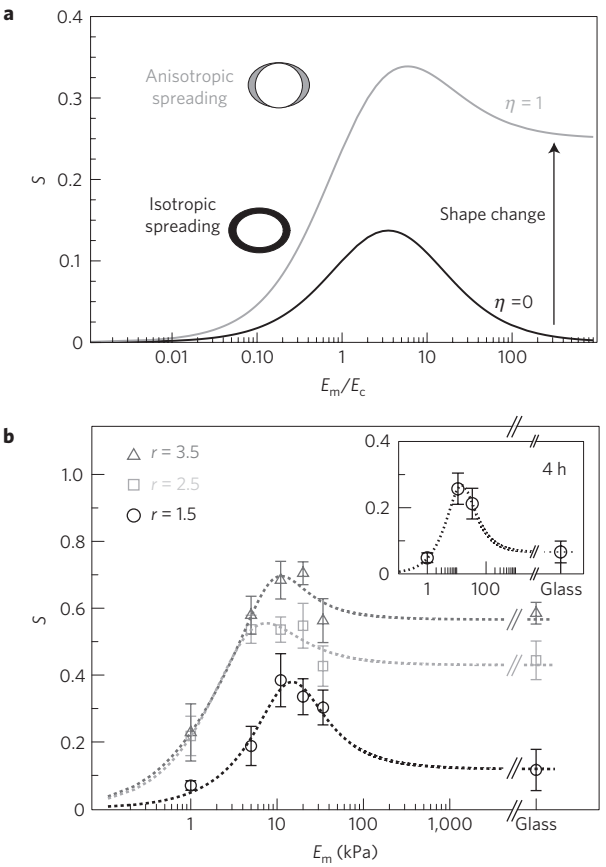

Figure 4 | The effect of axial cell elongation on stress-fibre polarization and experimental values of the order parameter *S* for different elastic substrates. a, A calculation of the 2D order parameter as a function of the matrix rigidity, for two cases: the cell spreads isotropically on the substrate, $\eta = 0$ (black curve); the cell spreads anisotropically on the substrate, $\eta = 1$ (grey curve), see the text. The two illustrations left of the curves show top views over the cell, before (shown as blank) and after (shown as shaded) cell spreading. In the asymmetric spreading case, r corresponds to the cell shape in an infinitely rigid matrix. For both curves we used $r = 2, \alpha = 2$ and Poisson ratios as in Fig. 3. **b**, The experimental values of the stress-fibre order parameter, $S = \langle\cos 2\theta\rangle$, 24 h after plating the cells, for the three groups of cells (of aspect ratios $r = 1.5, 2.5, 3.5$) as a function of Young's modulus of the matrix, E_m; θ is the angle between each stress fibre in the cell and the long axis of the fitted ellipse. Within each of the different groups, S is maximal for $E_m = 11$ kPa and generally increases with aspect ratio r, in agreement with our theoretical predictions. The error bars denote the standard error of the mean and theory curves (dotted lines) calculated from the simplified expansion of S (Supplementary Information) are shown to guide the eye.

After 24 h, both the morphology of the cells and cytoskeletal organization are significantly different ($p < 0.05$) on the substrates of 1, 11 and 34 kPa. Figure 1b,e shows that cells on the 11 kPa substrate, which has a rigidity comparable to that of the cells, show an elongated, spindle-like morphology and a closer alignment of the stress fibres with the long axis of the cell, as predicted by our model. In contrast, the cells on the 1 kPa (Figure 1a,d) and 34 kPa (Figure 1c,f) substrates are more isotropic in their overall shape and their stress fibres are less well aligned with the long axis of the cell.

Figure 4b shows the mean values of the order parameter, S, for different substrate elasticities E_m, 24 h after the cells were plated on the substrate. As a result of the natural variation of the shape of the cells, we regrouped the cells for each matrix elasticity E_m according

Table 1 | Order parameter S and standard error of the mean (s.e.m.) for cell groups of different aspect ratios r on substrates of different elasticities E_m.

E_m	1 kPa $S \pm$ s.e.m.	5 kPa $S \pm$ s.e.m.	11 kPa $S \pm$ s.e.m.	20 kPa $S \pm$ s.e.m.	34 kPa $S \pm$ s.e.m.	Glass $S \pm$ s.e.m.
$r = 1.5$	0.07 ± 0.01	0.19 ± 0.06	0.38 ± 0.08	0.33 ± 0.05	0.30 ± 0.05	0.12 ± 0.06
$r = 2.5$	0.22 ± 0.06	0.54 ± 0.04	0.54 ± 0.04	0.55 ± 0.07	0.43 ± 0.06	0.44 ± 0.06
$r = 3.5$	0.23 ± 0.09	0.58 ± 0.06	0.68 ± 0.06	0.70 ± 0.03	0.56 ± 0.07	0.58 ± 0.03

to their different aspect ratios $r = 1.5, 2.5$ and 3.5. For each of these subgroups, the order-parameter plots show a non-monotonic dependence on the matrix rigidity and in general S is higher for cells with a higher aspect ratio r. The non-monotonic dependence however is most pronounced for cells with a low aspect ratio, $r = 1.5$. For the groups with a higher aspect ratio, the curves saturate to higher values. This is likely to reflect the axial stress resulting from the concurrent cell elongation, as predicted by our model. Our simplified models thus capture the correct qualitative behaviour of stress-fibre polarization in stem cells as seen in Figs 3 and 4. Our findings thus suggest a mechanism that allows stem cells to adopt different internal structures in different mechanical environments and may provide a physical basis for the mechanosensitivity of stem-cell differentiation[7].

Methods

Elastic polyacrylamide gels with Young's elastic moduli E_m of 1, 5, 11, 20 and 34 kPa were prepared as reported elsewhere[7,35,36]. In addition, hyaluronic acid gels with a stiffness of 5 and 20 kPa and glass slides were prepared as described earlier[7]. The elasticity of the matrix was verified by force indentation measurements with an atomic force microscope (MFP-3D, Asylum Research) using a modified Hertz model. We carried out force indentation curves at 10 different spots (10 curves each) to ensure a homogeneous elastic modulus E_m throughout the whole gel. For cell adhesion, collagen type I (rat tail, BD Biosciences) was covalently attached to the hydrogels and to amino-silane-coated glass with the bifunctional crosslinker Sulfo-SANPAH (Pierce) assuring the same ligand density on substrates of different stiffnesses. Scanning force microscopy of the surface after coating revealed a homogeneous smooth surface without structured inhomogeneities. hMSCs, obtained from Lonza, were cultured in standard tissue-culture-treated plastic flasks (Corning) using MSC growth medium (low-glucose DMEM (Invitrogen) supplemented with 10% fetal bovine serum (Sigma) and 1% penicillin/streptomycin (Invitrogen)). Cells were plated on the substrates at 500 cells cm^{-2} to ensure sparse cultures. For immunostaining and imaging, the cells were fixed with a 10% solution of formaldehyde (Sigma) in PBS and subsequently permeabilized with a 0.5% solution of Triton X 100 (Sigma) in PBS. NMMIIa was immunostained with a primary antibody produced in rabbit (Sigma) followed by a secondary antibody (Alexa Fluor 488 donkey anti-rabbit IgG, Invitrogen) and F-actin was visualized using rhodamine phalloidin (Fluka). The nucleus was stained with a Hoechst stain (no. 33342, Invitrogen). Fluorescence images were taken on an inverted microscope (IX 71, Olympus) equipped with a $\times 20$ phase-contrast objective using a $\times 1.6$ post-magnification lens. To obtain unbiased cell images, single nuclei were located that looked healthy and had no close neighbours. Only then actin and NMMIIa images were taken. Supplementary Fig. S1 shows a composite fluorescence image (A) and the raw fluorescence intensity image of NMMIIa (B) that is used to determine cytoskeletal organization. To obtain sufficient statistics at least 60 cells per condition were analysed.

Image analysis. Cell area, orientation and the long and short axes of the cell were computed from the moments up to the second order of the thresholded binary image of the cell using NIH ImageJ[37]; the aspect ratio r is the ratio of the long axis to the short axis.

Segmentation and orientation analysis of cell stress fibres was carried out using a custom automated image analysis algorithm written in Mathematica (Wolfram Research). The segmentation uses a series of elongated Laplace of Gaussian (eLoG) kernels[38]. These are generated from n anisotropic Gaussians of the form

$$G = \frac{1}{2\pi\sigma_x\sigma_y} \exp\left(-\left(\frac{x^2}{2\sigma_x} + \frac{y^2}{2\sigma_y}\right)\right)$$

that are each rotated in steps of π/n, where n goes from 0 to $\pi - \pi/n$. For the results presented here we used $n = 15$. The Gaussian kernels are then convolved with a Laplacian filter given by

$$L = \begin{pmatrix} 0 & -1 & 0 \\ -1 & 4 & -1 \\ 0 & -1 & 0 \end{pmatrix}$$

The n eLoG kernels are each convolved with the original images producing n response images. The maximum over the n response images at each xy pixel is then used to create a single maximum response image. The segmentation shown in Supplementary Fig. S1C is the maximum response image after it has been thresholded using the Otsu method[39], which determines a threshold based only on the image intensity histogram and so does not introduce any experimenter bias. Finally, connected circular spots with a diameter greater than 10 pixels are removed from the thresholded image to reduce the contribution of bright non-fibrous points in the original image that lead to isotropic spots to the filtered image because the response of each eLoG kernel survives the threshold if the intensity in the original image is sufficiently high. The rotation angle of the filter that gave the maximum response at each pixel is taken as that pixel's orientation and is represented as the different colours. The average fibre orientation and order parameter are determined from the histogram of the individual pixel orientations.

To compare the alignment of the stress fibres for a single cell shape, the cells were regrouped according to their aspect ratios and the averaged orientational order parameter of the stress fibres S has been determined for each of these groups. These values are plotted in Fig. 4b and are listed in Table 1.

To determine the amount of NMMIIa, we used thresholded binary images of the determined stress fibres as a mask for the fluorescence images of NMMIIa. The total intensity after multiplication of the mask with the fluorescence image gives an estimate of the active contractile NMMIIa in stress fibres without including the diffuse background intensity from cytosolic NMMIIa. This is a measure of the total amount of contractile dipoles in the cell that increases with increasing substrate stiffness (see Supplementary Fig. S3).

Received 22 January 2009; accepted 4 February 2010; published online 21 March 2010

References

1. O'Neill, C., Jordan, P. & Ireland, G. Evidence for two distinct mechanisms of anchorage stimulation in freshly explanted and 3t3 swiss mouse fibroblasts. *Cell* **44,** 489–496 (1986).
2. Chen, C. S., Mrksich, M., Huang, S., Whitesides, G. M. & Ingber, D. E. Geometric control of cell life and death. *Science* **276,** 1425–1428 (1997).
3. McBeath, R., Pirone, D. M., Nelson, C. M., Bhadriraju, K. & Chen, C. S. Cell shape, cytoskeleton tension, and RoHA regulate stem cell lineage commitment. *Dev. Cell* **6,** 483–495 (2004).
4. Engler, A. J. *et al.* Myotubes differentiate optimally on substrates with tissue-like stiffness: Pathological implications for soft or stiff microenvironments. *J. Cell Biol.* **166,** 877–887 (2004).
5. Yeung, T. *et al.* Effects of substrate stiffness on cell morphology, cytoskeletal structure, and adhesion. *Cell Motil. Cytoskeleton* **60,** 24–34 (2005).
6. Discher, D. E., Janmey, P. & Wang, Y. Tissue cells feel and respond to the stiffness of their substrate. *Science* **310,** 1139–1143 (2005).
7. Engler, A. J., Sen, S., Sweeney, H. L. & Discher, D. E. Matrix elasticity directs stem cell lineage specification. *Cell* **126,** 677–689 (2006).
8. Georges, P. C., Miller, W. J., Meaney, D. F., Sawyer, E. S. & Janmey, P. A. Matrices with compliance comparable to that of brain tissue select neuronal over glial growth in mixed cortical cultures. *Biophys. J.* **90,** 3012–3018 (2006).
9. Cai, Y. *et al.* Cytoskeletal coherence requires myosin-IIA contractility. *J. Cell Sci.* **123,** 413–423 (2010).
10. Bhattacharya, D., Talwar, S., Mazumder, A. & Shivashankar, G. V. Spatio-temporal plasticity in chromatin organization in mouse cell differentiation and during drosophila embryogenesis. *Biophys. J.* **96,** 3832–3839 (2009).
11. Wang, N., Tytell, J. D. & Ingber, D. E. Mechanotransduction at a distance: Mechanically coupling the extracellular matrix with the nucleus. *Nat. Rev. Mol. Cell Biol.* **10,** 75–82 (2009).

12. Bershadsky, A., Kozlov, M. & Geiger, B. Adhesion-mediated mechanosensitivity: A time to experiment, and a time to theorize. *Curr. Opin. Cell Biol.* **18,** 472–481 (2006).
13. Iba, T. & Sumpio, B. Morphological response of human endothelial cells subjected to cyclic strain *in vitro*. *Microvasc. Res.* **42,** 245–254 (1991).
14. Rodriguez, J. P., Gonzalez, M., Rios, S. & Cambiazo, V. Cytoskeletal organization of human mesenchymal stem cells (msc) changes during their osteogenic differentiation. *J. Cell. Biochem.* **93,** 721–731 (2004).
15. Curtis, A., Aitchison, G. & Tsapikouni, T. Orthogonal (transverse) arrangements of actin in endothelia and fibroblasts. *J. R. Soc. Interface* **3,** 753–756 (2006).
16. Ghibaudo, M. *et al*. Traction forces and rigidity sensing regulate cell functions. *Soft Matter* **4,** 1836–1843 (2008).
17. Kumar, S. *et al*. Viscoelastic retraction of single living stress fibres and its impact on cell shape, cytoskeletal organization, and extracellular matrix mechanics. *Biophys. J.* **90,** 3762–3773 (2006).
18. Dubin-Thaler, B. J. *et al*. Quantification of cell edge velocities and traction forces reveals distinct motility modules during cell spreading. *PLOS One* **3,** e3735 (2008).
19. Griffin, M. A. *et al*. Patterning, prestress, and peeling dynamics of myocytes. *Biophys. J.* **86,** 1209–1222 (2004).
20. Wang, N. *et al*. Cell prestress. i. Stiffness and prestress are closely associated in adherent contractile cells. *Am. J. Physiol. Cell Physiol.* **282,** C606–C616 (2002).
21. Wang, N., Ostuni, E., Whitesides, G. M. & Ingber, D. E. Micropatterning tractional forces in living cells. *Cell Motil. Cyto.* **52,** 97–106 (2002).
22. Chicurel, M. E., Chen, C. S. & Ingber, D. E. Cellular control lies in the balance of forces. *Curr. Opin. Cell Biol.* **10,** 232–239 (1998).
23. Balaban, N. Q. *et al*. Force and focal adhesion assembly: A close relationship studied using elastic micropatterned substrates. *Nature Cell Biol.* **3,** 466–472 (2001).
24. Schwarz, U. S., Erdmann, T. & Bischofs, I. B. Focal adhesions as mechanosensors: The two-spring model. *Biosystems* **83,** 225–232 (2006).
25. Grinnell, F. Fibroblast-collagen-matrix contraction: Growth-factor signalling and mechanical loading. *Trends Cell Biol.* **10,** 362–365 (2000).
26. Eshelby, J. D. The determination of elastic field of an ellipsoidal inclusion, and related problems. *Proc. R. Soc. A* **241,** 376–396 (1957).
27. Mura, T. *Micromechanics of Defects in Solids* (Kluwer Academic, 1991).
28. Landau, L. D. & Lifshitz, E. M. *Theory of Elasticity* 3rd edn (Course of Theoretical Physics, Vol. 7, Reed Educational and Professional Publishing, 1986).
29. Jaswon, M. A. & Bhargava, R. D. Two-dimensional elastic inclusion problems. *Proc. Camb. Phil. Soc.* **57,** 669–680 (1961).
30. Siems, R. Mechanical interactions of point defects. *Phys. Status Solidi* **30,** 645–658 (1968).
31. Schwarz, U. S. & Safran, S. A. Elastic interactions of cells. *Phys. Rev. Lett.* **88,** 048102 (2002).
32. Carlsson, A. E. Contractile stress generation by actomyosin gels. *Phys. Rev. E* **74,** 051912 (2006).
33. Riveline, D. *et al*. Focal contacts as mechanosensors: Externally applied local mechanical force induces growth of focal contacts by an mdia1-dependent and rock-independent mechanism. *J. Cell Biol.* **153,** 1175–1185 (2001).
34. Schwarz, U. S. & Bischofs, I. B. Physical determinants of cell organization in soft media. *Med. Eng. Phys.* **27,** 763–772 (2005).
35. Pelham, R. J. & Wang, Y. L. Cell locomotion and focal adhesions are regulated by substrate flexibility. *Proc. Natl Acad. Sci. USA* **94,** 13661–13665 (1997).
36. Engler, A. J., Rehfeldt, F., Sen, S. & Discher, D. E. *Microtissue Elasticity: Measurements by Atomic Force Microscopy and its Influence on Cell Differentiation* Vol. 83, 521–545 (Academic, 2007).
37. Rasband, W. S. ImageJ US National Institute of Health, Bethesda, Maryland, USA, <http://rsb.info.nih.gov/ij/>, 1997–2007.
38. Haralick, R. & Shapiro, L. *Computer and Robot Vision* Vol. 1 (Addison-Wesley, 1992).
39. Otsu, N. Threshold selection method from grey-level histograms. *IEEE Trans. Syst. Man Cybernetics* **9,** 62–66 (1979).

Acknowledgements

We thank R. De, R. Paul and N. Gov for many useful discussions. We are grateful to the Israel Science Foundation, the Clore Center for Biological Physics, the Schmidt Minerva Center and an EU Network grant for their support. F.R. gratefully acknowledges financial support through the Feodor Lynen fellowship of the Alexander von Humboldt Foundation. D.E.D. thanks NFS and NIH. A.E.X.B. was supported by a scholarship from the Natural Sciences and Engineering Research Council of Canada.

Author contributions

A.Z. and S.A.S. developed the theory. F.R., A.E.X.B. and D.E.D. designed the experiments; F.R. carried out the experiments; A.E.X.B. wrote the image analysis algorithm. All authors analysed the data and wrote the paper.

Additional information

The authors declare no competing financial interests. Supplementary information accompanies this paper on www.nature.com/naturephysics. Reprints and permissions information is available online at http://npg.nature.com/reprintsandpermissions. Correspondence and requests for materials should be addressed to A.Z.